Analyzing the role of pulse density and voxelization parameters on full-waveform LiDAR-derived metrics

Crespo-Peremarch, Pablo [1,2*], Ruiz, Luis Ángel [1,2], Balaguer-Beser, Ángel [1,3] and Estornell, Javier [1,2]

[1] Geo-Environmental Cartography and Remote Sensing Group (CGAT), Universitat Politècnica de València, Camí de Vera s/n, 46022, València, Spain.

[2] Department of Cartographic Engineering, Geodesy and Photogrammetry, Universitat Politècnica de València, Camí de Vera s/n, 46022, València, Spain.

[3] Department of Applied Mathematics, Universitat Politècnica de València, Camí de Vera s/n, 46022, València, Spain.

Keywords: airborne laser scanning, voxelization, voxel size, assignation value, side-lap effect.

Abstract

LiDAR full-waveform (L_{FW}) pulse density is not homogeneous along study areas due to overlap between contiguous flight stripes and, to a lesser extent, variations in height, velocity and altitude of the platform. As a result, L_{FW}-derived metrics extracted at the same spot but at different pulse densities differ, which is called "side-lap effect". Moreover, this effect is reflected in forest stand estimates, since they are predicted from L_{FW}-derived metrics. This study was

[*] Corresponding author
Email address: pabcrepe@cgf.upv.es

undertaken to analyze L_{FW}-derived metric variations according to pulse density, voxel size and value assignation method in order to reduce the side-lap effect. Thirty LiDAR samples with a minimum density of 16 pulses·m^{-2} were selected from the testing area and randomly reduced to 2 pulses·m^{-2} with an interval of 1 pulse·m^{-2}, then metrics were extracted and compared for each sample and pulse density at different voxel sizes and assignation values. Results show that L_{FW}-derived metric variations as a function of pulse density follow a negative exponential model similar to the exponential semivariogram curve, increasing sharply until they reach a certain pulse density, where they become stable. This value represents the minimum pulse density (MPD) in the study area to optimally minimize the side-lap effect. This effect can also be reduced with pulse densities lower than the MPD modifying L_{FW} parameters (i.e. voxel size and assignation value). Results show that L_{FW}-derived metrics are not equally influenced by pulse density, such as number of peaks (NP) and ROUGHness of the outermost canopy (ROUGH) that may be discarded for further analyses at large voxel sizes, given that they are highly influenced by pulse density. In addition, side-lap effect can be reduced by either increasing pulse density or voxel size, or modifying the assignation value. In practice, this leads to a proper estimate of forest stand variables using L_{FW} data.

1. Introduction

LiDAR technologies have been widely used on forest applications during the last decades. Discrete LiDAR (L_D) is the most common LiDAR data. Its success for estimating forest stand variables and classifying fuel models has been proven in several studies (Lim et al., 2003; Bortolot and Wynne, 2005; Mutlu et al., 2008; Ruiz et al., 2018; Guerra-Hernández et al., 2016; Hevia et al., 2016). LiDAR full-waveform (L_{FW}) has also been used for estimating forest stand variables (Cao et al., 2014; Hermosilla et al., 2014a), classifying tree species (Reitberger et al., 2008; Heinzel and Koch, 2011; Cao et al., 2016) and segmenting single trees (Reitberger et al., 2009). L_{FW} registers the complete signal emitted from the system and backscattered from different vertical layers (Mallet and Bretar, 2009). The amplitude of the waveform in each bin is related to the physical properties of the object reached (Song et al., 2002; Guo et al., 2011; Hermosilla et al., 2014a) and to the angle of incidence (Kukko et al., 2008). Therefore, compared to the L_D, it provides more information about the vertical distribution of the vegetation. However, L_{FW} processing is more complex and time consuming, so it has been used much less frequently than L_D.

Both L_D and L_{FW} usually present heterogeneous pulse densities along the studied areas. This is due to the fact that side-lap areas, where two or more flight lines overlap, have higher pulse densities. These pulse density variations affect L_D-derived metrics and the subsequent forest variables estimates and maps. Thus, a L_D-derived metric may have different values in two samples with identical forest features but different pulse densities. Given that L_D-derived metrics are used in regression models to estimate forest stand variables, the values of these variables will be influenced as well.

The influence of L_D pulse density on forest stand variable estimates was analyzed in several studies (Table 1). All of these studies present variations in forest stand estimates, however, since they were focused on different ecosystems and used different ranges of pulse densities, variations have different scales. Gobakken and Naesset (2008), Magnussen et al. (2010) and Jakubowski et al. (2013) observed that estimated variables were not significantly affected by density until dropping 0.25 points.m^{-2} in the first study, and 1 pulse·m^{-2} in the last two. Analyzing specific groups of variables, Magnussen et al. (2010), González-Ferreiro et al. (2012), Strunk et al. (2012), Treitz et al. (2012), Jakubowski et al. (2013) and Varo-Martínez et al. (2017) did not find significant influence of pulse density on variables related to height, such as: mean, dominant, tree and Lorey's height, and mean height to live crown. According to Strunk et al. (2012) and Treitz et al. (2012), variables related to tree density (i.e. number of stems and stem density) were not significantly affected either, however, Magnussen et al. (2010) observed on the reliability ratio that stem density was affected using low pulse densities. The reliability ratio was defined by Hansen et al. 2015 as the variance of a metric among sample plots divided by the total variance of the metric (i.e. the variance among sample plots plus the average variance within the plot). Regarding variables related to trunk size, such as quadratic mean diameter (Treitz et al., 2012), diameter at breast height (Jakubowski et al., 2013), and basal area (Magnussen et al., 2010; González-Ferreiro et al., 2012; Stunk et al., 2012; Treitz et al., 2012; Jakubowski et al., 2013; Ruiz et al., 2014; Varo-Martínez et al., 2017), had no significant differences between different pulse densities, except for the basal area in a tropical forest in a study carried out by Manuri et al. (2017). Among volume variables (i.e. volume over bark, stem volume, gross total and merchantable volume), only volume over bark in González-Ferreiro et al. (2012) was significantly affected by pulse density variations. Additionally, Jakubowski et al. (2013) for shrub cover and height variables, Ruiz et al. (2014) for canopy cover, and Silva et al. (2017) for aboveground carbon, observed that they were not significantly affected either. Lastly, stem biomass and aboveground biomass were influenced by L_D pulse density in an Atlantic and a Tropical forest (González-Ferreiro et al., 2012; Manuri et al., 2017), but Treitz et al. (2012) did not find significant differences in aboveground biomass in a Boreal forest using different densities. Overall, aboveground biomass is more influenced by pulse density than height variables, although another factor affecting tree density, basal area and volume is the type of ecosystem.

While the influence of pulse density on forest stand variables estimated from L_D-derived metrics has been widely studied in different ecosystems, less attention has been paid to how L_D-derived metrics are influenced. Roussel et al. (2017) mentioned that even when the values of estimated variables are stable for different pulse densities, L_D-derived metrics are affected, since they are measures and are not statistically fitted. Gobakken and Naesset (2008) and other authors, such as Hansen et al. (2015) and Roussel et al. (2017), analyzed the effects of pulse density on L_D-derived metrics. The first study computed height (e.g. percentiles, maximum, mean and coefficient of variation) and density metric differences between the initial point density (i.e. 1.13 points.m^{-2}) and thinned data (i.e. 0.25, 0.13 and 0.06 points.m^{-2}) at different sample sizes. They observed that the maximum height metric had large variations between point densities, these variations being even larger when point density decreased. The remaining metrics did not have a clear pattern. Hansen et al. (2015) computed seven L_D-derived metrics: mean, maximum, variance, percentiles 10 and 90 of the above ground heights, and the proportion of points above the ground and above the mean. They observed that most of the metrics were not influenced by pulse densities, except for the maximum elevations that decreased with lower pulse densities. However, the reliability ratio increased for all metrics when pulse density increased until reaching a threshold where it remained stable. A possible explanation for this might be that mean values of L_D-derived metrics did not vary much due to pulse density. In contrast, the standard deviation increased for lower pulse densities, and hence the reliability ratio varied as well.

Roussel et al. (2017) also analyzed how maximum height varied for different pulse densities. They concluded that metric variations were not only subject to pulse density, but additionally to LiDAR footprint size and canopy shape. The flatter the top canopy (i.e. fewer singularities), the lesser difference between pulse densities.

Table 1. Summary of existing studies about the influence of discrete LiDAR pulse density on forest stand estimates.

Study	Study Area	Ecosystem	Highest (HD) - lowest (LD) densities (pulses˙m^{-2})	Estimated variables	Results: HD-LD
Gobakken and Naesset (2008)	Våler, Southeastern Norway	Boreal forest	1.13 – 0.06 points.m^{-2}	Hl: Lorey's height BA: basal area Vol: stand volume	Estimate differences: Hl ≈ 0.2-0.6 m BA ≈ 0.0-2.5 m^2.ha-1 Vol ≈ 5-30 m^2.ha-1
Magnussen et al. (2010)	Aurskog-Høland, Southeastern Norway	Boreal forest	2 – 0.25	Hl: Lorey's height BA: basal area V: volume over bark SD: stem density	R^2 (%): BA ≈ 79-72 V ≈ 85-80 Reliability ratio: Hl ≈ 1.0-0.9 BA ≈ 0.98-0.95 V ≈ 0.96-0.92 SD ≈ 0.96-0.81
González-Ferreiro et al. (2012)	Galicia, Northwestern Spain	Atlantic forest	8 – 0.5	Hm: mean height Hd: dominant height BA: basal area V: volume over bark Wcr: crown biomass Wst: stem biomass AGB: aboveground biomass	R^2 (%): Hm = 78.6-75.9 Hd = 84.6-86.5 BA = 67.8-69.2 V = 69.1-79.4 Wcr = 68.7-68.8 Wst = 73.2-82.7 AGB = 74.6-80.4
Strunk et al. (2012)	Western Washington State, USA	Humid temperate – Pacific lowland mixed forest	3 – 0.05	ST: number of stems	nRMSE (%): ST ≈ 56-57
Treitz et al. (2012)	Ontario, Canada	Boreal forest	3.2 – 0.5	Hm: mean height TH: tree height QMD: quadratic mean diameter BA: basal area GTV: gross total volume GMV: gross merchantable volume AGB: aboveground biomass SD: stem density	R^2 (%): Black spruce (BS), Intolerant hardwood (IH). Hm = 95.1-93.6 (BS); 76.7, 77.3 (IH) TH = 92.3, 90.3 (BS); 94.1, 94.3 (IH) QMD = 83.8, 86.3 (BS); 84.2, 84.0 (IH) BA = 91.8, 93.5 (BS); 83.7, 82.3 GTV = 94.9, 94.2 (BS); 83.7, 82.3 (IH) GMV = 91.6, 93.9 (BS); 87.3, 87.7 (IH) AGB = 92.5, 93.2 (BS); 78.8, 77.5 (IH) SD = 88.8, 86.1 (BS); 23.9, 24.8 (IH)

Table 1 (cont.). Summary of existing studies about the influence of discrete LiDAR pulse density on forest stand estimates.

Study	Study Area	Ecosystem	Highest (HD) - lowest (LD) densities (pulses˙m^{-2})	Estimated variables	Results: HD-LD
Jakubowski et al. (2013)	Tahoe National Forest. Northern California, USA	Mediterranean-climate forest	9 – 0.01	TH: tree height HTLCB: mean height lo live crown base BA: basal area DBH: diameter at breast height SC: shrub cover SH: shrub height	R^2 (%): TH = 86.8-52.4 HTLCB = 76.8-28.8 BA = 77.5-48.9 DBH = 59.7-38.0 SC = 53.1-11.9 SH = 45.9-29.0
Ruiz et al. (2014)	La Serranía de Cuenca, Central Spain	Mediterranean mountain forest	6 - 0.25 points.m^{-2}	V: volume AGB: aboveground biomass BA: basal area CC: canopy cover	R^2 (%) (with a plot radius of 16 m): V ≈ 90.5-86.0 AGB ≈ 85.5-82.0 BA ≈ 87.0-83.0 CC ≈ 89.0-89.0
Manuri et al. (2017)	Central Kalimantan, Indonesia	Tropical forest	2.8 – 0.01 points.m^{-2}	AGB: aboveground biomass BA: basal area	R^2 (%): AGB ≈ (90.0)-(80.0,60.0) BA ≈ (90.0)-(70.0,40.0)
Silva et al. (2017)	Paraíba Valley, São Paulo, Brazil	Humid subtropical forest	10 - 5	AGC: aboveground carbon	R^2 (%): AGC = 82.17-81.79
Varo-Martínez et al. (2017)	Sierra de Los Filabres, Southeastern Spain	Semi-arid Mediterranean forest	10 – 0.5	Hd: dominant height BA: basal area	R^2 (%): Hd = (97.0,94.0)-(95.0,93.0) BA = (92.0,88.0)-(93.0,87.0)

Differences in data characteristics between L_D and L_{FW} requires different pre-processing. While L_D-derived metrics can be recomputed by simply varying the number of points (i.e. pulse density), L_{FW} data pre-processing is more complex and there are other parameters that may also be considered. This complexity can explain why the influence of pulse density on L_{FW}-derived metrics and forest stand variable estimates has received less attention (Crespo-Peremarch et al., 2016). Furthermore, few published studies have analyzed the evolution of FW-derived metrics by artificially reducing the pulse density. Crespo-Peremarch et al. (2016) observed L_{FW}-derived metric differences (namely “side-lap effect”) in adjacent areas that were compared pairwise, with similar forest features but having different densities. It was found that L_{FW}-derived metrics were influenced by density variations caused by flight stripe side-lap areas. A standard pre-processing method for L_{FW}-derived metric extraction is voxelization (Hermosilla et al., 2014b). LiDAR return pulses are clustered into voxels (e.g. rectangular prisms), whose values are computed as the statistics (i.e. maximum, mean, median, etc.) of return pulse amplitude values of waveforms within the voxels. These voxel columns of values from the top tree to the ground describe the pseudo-vertical waveform, which corrects the registered scan angle (Hermosilla et al., 2014b). Once pseudo-vertical waveform is generated, L_{FW}-derived metrics can be extracted. Changing the voxel size and the assignation value may diminish the side-lap effect without modifying the pulse density. As mentioned above, increasing the voxel size reduces the number of empty voxels, avoiding gaps in the pseudo-vertical waveforms. On the other hand, changing the assignation value can avoid outliers from amplitude values, which is more likely when the voxel size increases.

Crespo-Peremarch et al. (2016) and Crespo-Peremarch and Ruiz (2018) observed that the side-lap effect in L_{FW}-derived metrics had an effect on forest stand variable estimates as well, given that the latter are estimated through L_{FW}-derived metrics. The first study visually observed these differences for a large area, while the latter observed that R^2 values of aboveground biomass and canopy base height between different pulse densities differed by 3% and 5%, respectively, for a voxel size of 0.25 m. Therefore, forest stand variables were wrongly mapped with the side-lap effect due to pulse density variation. Therefore, correcting side-lap effect is essential to properly estimate forest stand variables. Comparing L_{FW}-derived metrics obtained using different pulse densities may help to better understand how metrics are influenced and to reduce side-lap effect.

The aim of this paper is to analyze L_{FW}-derived metric variations when pulse density, voxel size and assignation value are modified. To do this, we randomly diminished pulse density from 16 to 2 pulses·m^{-2} every 1 pulse·m^{-2} in a set of 30 samples. In addition, for each density we computed six L_{FW}-derived metrics using five different assignation values (i.e. maximum, mean, median, percentiles 90 and 95) and voxel sizes from 0.25 to 1.55 m every 0.10 m. Moreover, the L_{FW}-derived metric values obtained at every pulse density for the different combinations of L_{FW} parameters was analyzed. Results will lead to a better understanding of the relation between L_{FW} methodological parameters and pulse density in order to improve the use of these data and techniques.

2. Methods

2.1. Study area

The study area (2,258 ha) is located in Panther Creek (Oregon, USA) (Fig. 1a), in the Cascade mixed forest ecoregion (Bailey, 1980). The dominant species is Douglas-fir (*Pseudotsuga menziesii*) very occasionally mixed with other conifers such as western red cedar (*Thuja plicata*), western hemlock (*Tsuga heterophylla*) and grand fir (*Abies grandis*), and broad-leaved species such as bigleaf maple (*Acer macrophyllum*) and red alder (*Alnus rubra*). Tree heights are variable due to harvesting, being up to 60 m. Altitudes in the total extent of the study area range from 100 to 700 m.

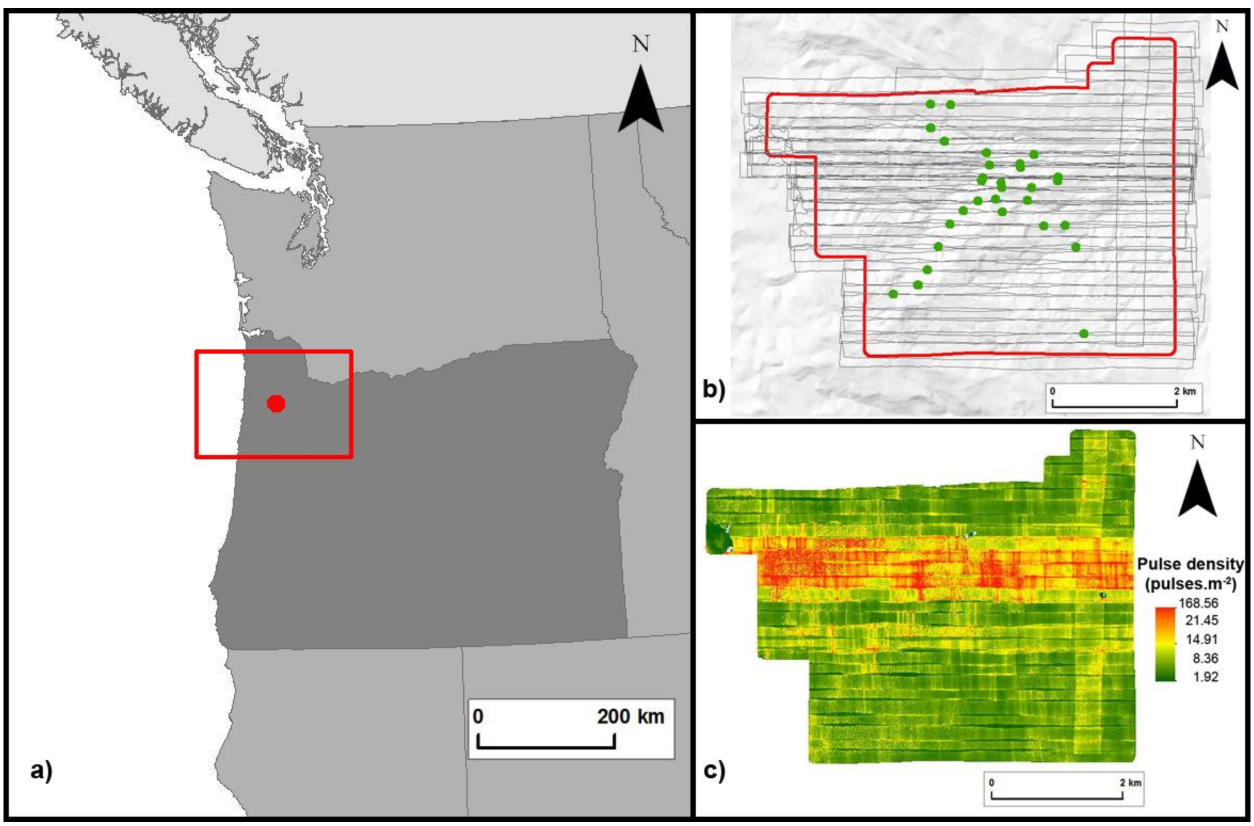

Fig. 1. (a) Study area location in the USA Pacific Northwest, (b) flight trajectories and sample locations (green) within the study area limits (red), and (c) pulse density.

2.2. LiDAR full-waveform Data

2.2.1. Data acquisition

L_{FW} data were acquired in July 2010 using a Leica ALS60 over 3,264.51 ha, with a pulse density ranging from 2 to 168 pulses·m^{-2}, and an average of 10.4 pulses·m^{-2} (Fig. 1c). Data were registered at an average flight altitude of 900 m above ground level, at 105 kHz pulse frequency, and with a scan angle of ±14º from nadir. The study area was covered with flight stripe side-lap of ≥ 50% (≥ 100% overlap). Waveform amplitudes were recorded in 256 bins with a temporal sample spacing of 2 ns (i.e. 0.3 m) and a footprint size of ≈ 0.25 m. In addition, a digital terrain model (DTM) with 1 m spatial resolution was provided by the company that registered L_{FW} data, and its vertical accuracy assessed using 33 GPS ground control points, obtaining a RMSE of 0.19 m.

2.2.2. Radiometric calibration and waveform denoising

The overall processing followed in this paper is described in Fig. 2, and this is as follows:

Radiometric calibration is an essential pre-processing step of L_{FW} data, since most of the metrics depend on the amplitude values. There are two main approaches of radiometric calibration: relative and absolute. While the former reduces radiometric differences between flight stripes without ground data, the latter reduces differences related to acquisition day conditions and sensors using target properties (Wagner, 2010). In this study, we applied a relative radiometric calibration, given that target properties from ground data were not available, and there were no paved roads with known radiometric values in the study area. Therefore, we corrected the amplitude values along the waveform using Eq. (1) described by Kashani et al. (2015) for nonextended objects, which corrects amplitude values taking into account the range from sensor to object and the local incidence angle.

$$A_C = A * \frac{{R_i}^3}{{R_{ref}}^3} * \frac{1}{\cos \alpha} \quad (1)$$

where A_C = corrected amplitude,

A = amplitude to be corrected,

R_i = range from the sensor to the object,

R_{ref} = reference range set to 1000 m for this study,

α = local incidence angle.

Once waveforms were radiometrically corrected, noise was still present. In order to remove it, we followed the denoising process described by Hermosilla et al. (2014b), consisting of applying a noise threshold defined as the mean plus four times the standard deviation of the waveform amplitude values (Lefsky et al., 2005), removing all lower values below the threshold. Additionally, a Gaussian filter was used to reduce any remaining noise.

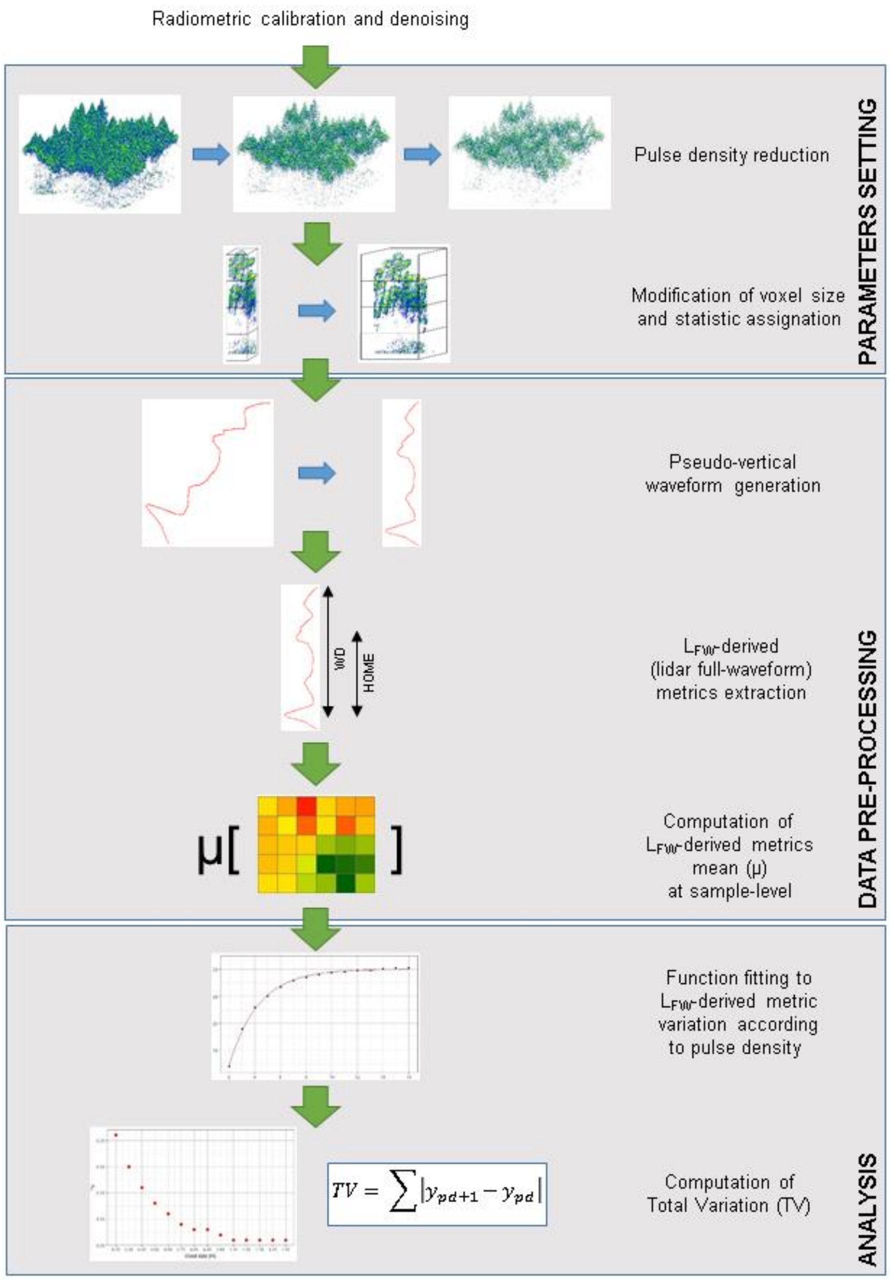

Fig. 2. Overall processing flowchart.

2.2.3. Sample selection and pulse density reduction

In order to carry out the analysis, a total of 30 samples were selected from the study area where conifers were dominant (Fig. 1b). These samples were located where pulse density was higher in order to be able to test a higher number of density variations. The polygon samples were squareshaped with an area of 804.25 m^2 each, this is the equivalent area of 16 m radius circular plots. The pulse density was reduced from 16 to 2 pulses·m^{-2} with an interval of 1 pulse·m^{-2}, resulting in 15 different density values. The initial pulse density was selected considering the maximum and common pulse density value found in the 30 plots.

Pulse density was reduced randomly (Fig. 2) (i.e. from 16 to 2 pulses·m^{-2} with an interval of 1 pulse·m^{-2}) and computed as the number of pulses contained in the polygon sample divided by the area. To reduce pulse density, we calculated the number of pulses (n) required in an area of 804.25 m^2 to obtain a pulse density equal to p. Then, n random pulses were kept for the analysis and the rest were discarded.

2.2.4. Metrics extraction

Once pulses were denoised and randomly filtered based on established pulse densities, a height normalization and a voxelization process from the waveform bins was carried out. The DTM described above and generated from the original pulse densities was used for height normalization. Regarding the voxelization process, we tested 14 voxel size variations in XY dimensions (Fig. 2): 0.25, 0.35, 0.45, 0.55, 0.65, 0.75, 0.85, 0.95, 1.05, 1.15, 1.25, 1.35, 1.45 and 1.55 m. The minimum voxel size was equal to the footprint size. The voxel size in Z dimension was not modified, and the vertical distance between waveform bins, based on the temporal sample spacing of the LiDAR system, was respected. Therefore, the voxel size in Z dimension was 0.3 m, equal to the temporal sample spacing. In addition, the voxel value was computed (Fig. 2) using five different statistics (maximum, mean, median, percentiles 90 and 95) for all the waveform bins within each voxel. As a result, every voxel had a value for these five statistics. Afterwards, each column of voxels was computed separately. Voxel values from the top tree to the ground describe a new waveform corrected from scan angle and called "pseudo-vertical" waveform (Hermosilla et al., 2014b) (Fig. 2). L_{FW}-derived metrics were extracted from the pseudo-vertical waveform (Fig. 2). The six L_{FW}-derived metrics used in this paper were introduced by Duong (2010): HOME, WD, NP, ROUGH, RWE and FS (Table 2).

Table 2. Description of L_{FW}-derived metrics used in this study.

Metric	Description
HOME	Height Of Median Energy: height where the median of the return energy is reached
WD	Waveform Distance: height from the ground to the beginning of the waveform
NP	Number of Peaks: number of peaks of the waveform
ROUGH	ROUGHness of outermost canopy: distance from the beginning of the waveform to the first peak
RWE	Return Waveform Energy: sum of waveform amplitudes
FS	Front Slope angle: vertical angle from the beginning of the waveform and the amplitude of the first peak

As a result, each column of voxels had a pseudo-vertical waveform, and therefore a value for each L_{FW}-derived metric. Finally, the L_{FW}-derived metric value for each sample was computed as the average of all the voxel columns within each polygon sample (Fig. 2).

2.3. Analysis of metrics variation

2.3.1. L_{FW}-derived metric variation related to pulse density

Once L_{FW}-derived metrics were computed for every sample, voxel size, assignation value and pulse density, we analyzed its variation related to the pulse density (Fig. 2). The goal was to analyze L_{FW}-derived metric variations modifying the three mentioned parameters (i.e. voxel size, assignation value and pulse density). We first observed the variation related to pulse density for several samples at different voxel sizes and assignation values. As this variation followed a negative exponential distribution, we used the least squares method to find the most appropriate parameter values, fitting a negative exponential model (Eq. (2)). In this model, based on the exponential semivariogram model (David, 1977), L_{FW}-derived metric values (y=dependent variable) tend to remain stable around a sill with a slight positive slope at a given pulse density (x=independent variable). The formula of the negative exponential function is as follows:

$$y = a + c * (1 - exp^{-\frac{3*x}{b}}) \quad (2)$$

where x = value of density in pulses·m^{-2},

y = value of the L_{FW}-derived metric,

a = value of y at which x=0 in the negative exponential model,

b = value of x where y reaches the 95% of the sill value,

c = range of y between a and the value of y at which the function is stabilized then,

$a + c = y$ value of the sill.

On the other hand, each sample has different values for L_{FW}-derived metrics, due to vegetation variability. Therefore, with the aim of working with all 30 samples we did not fit a function for all the samples together. Instead, we fit a function for each sample individually, and then we averaged the model results from the 30 samples clustered by L_{FW}-derived metric, voxel size and assignation value. As a result, we computed 12,600 different models (i.e. 30 samples × 6 L_{FW}-derived metrics × 14 voxel sizes × 5 assignation values) resulting 420 averaged results (i.e. 6 L_{FW}-derived metrics × 14 voxel sizes × 5 assignation values). Only negative exponential models with a convergence tolerance of < 1 x 10^{-5} in the iterative fitting process were used for the study. Validation was carried out using the Jackknife procedure described by Duda et al. (2012), which utilizes a leave-one-out procedure. Results were evaluated using the coefficient *b*, which shows the minimum pulse density where L_{FW}-derived metrics hardly vary, and the Jackknife bias, which shows the average of the deviations after removing one observation at each iteration.

2.3.2. L_{FW}-derived metric variation according to voxel size and assignation value

As seen in the previous section, analyzing variability of L_{FW}-derived metrics as pulse density increases provides the minimum pulse density (MPD) where metrics stay steady, corresponding to the coefficient *b* of the negative exponential model. In addition, analyzing the variability using different voxel sizes and assignation values may help to diminish the influence of the pulse density (Crespo-Peremarch et al., 2016). Total Variation (TVar) (Eq. (3)) (Harten, 1983) can be used instead of the variability of L_{FW}-derived metric values for the different pulse densities (Fig. 2), explained in the previous section. The TVar computes the sum of differences between adjacent values. Hence, the lower the TVar value, the less variability the L_{FW}-derived metric has due to the pulse density. The formula of the TVar is as follows:

$$TVar = \sum_{pd=2}^{16-1} \left| y_{pd+1} - y_{pd} \right| \tag{3}$$

where y = value of the metric in a given pulse density (*pd*) and,

pd = pulse density.

Given that L_{FW}-derived metrics and assignation values have, in practice, a different range of values, L_{FW}-derived metrics were rescaled independently for each possible combination of metric and assignation type. A modified version of the feature scaling method was used (Eq. (4)) to standardize data. In our case, the minimum value was equal to zero, since we wanted to keep the minimum TVar value as zero:

$$y = \frac{x - \min(x)}{\max(x) - \min(x)} \;/\; \min(x) = 0 \qquad (4)$$

where y = standardization of the L_{FW}-derived metric value,

x = L_{FW}-derived metric value,

min(x) = minimum L_{FW}-derived metric value grouped by L_{FW}-derived metric and assignation value, in our case modified to min(x) = 0,

max(x) = maximum L_{FW}-derived metric value grouped by L_{FW}-derived metric and assignation value.

Afterwards, we computed the TVar from the 30 samples by averaging every L_{FW}-derived metric, voxel size and assignation value.

3. Results

Fig. 3 shows how the pseudo-vertical waveform and the L_{FW}-derived metrics from the same voxel column vary modifying the pulse density, voxel size and assignation value. The lower the pulse density, the more null values and the less detail appear in the pseudo-vertical waveform.

However, changes in the waveform due to pulse density reduction seem to be less noticeable when voxel size increases to 1.25 m, except for the median assignation value. In addition, pseudo-vertical waveforms using the median assignation are smoother than those using the maximum assignation.

Analyzing L_{FW}-derived metric values for the same voxel size, HOME, WD, ROUGH and FS do not show significant variations. On the contrary, NP and RWE are more variable.

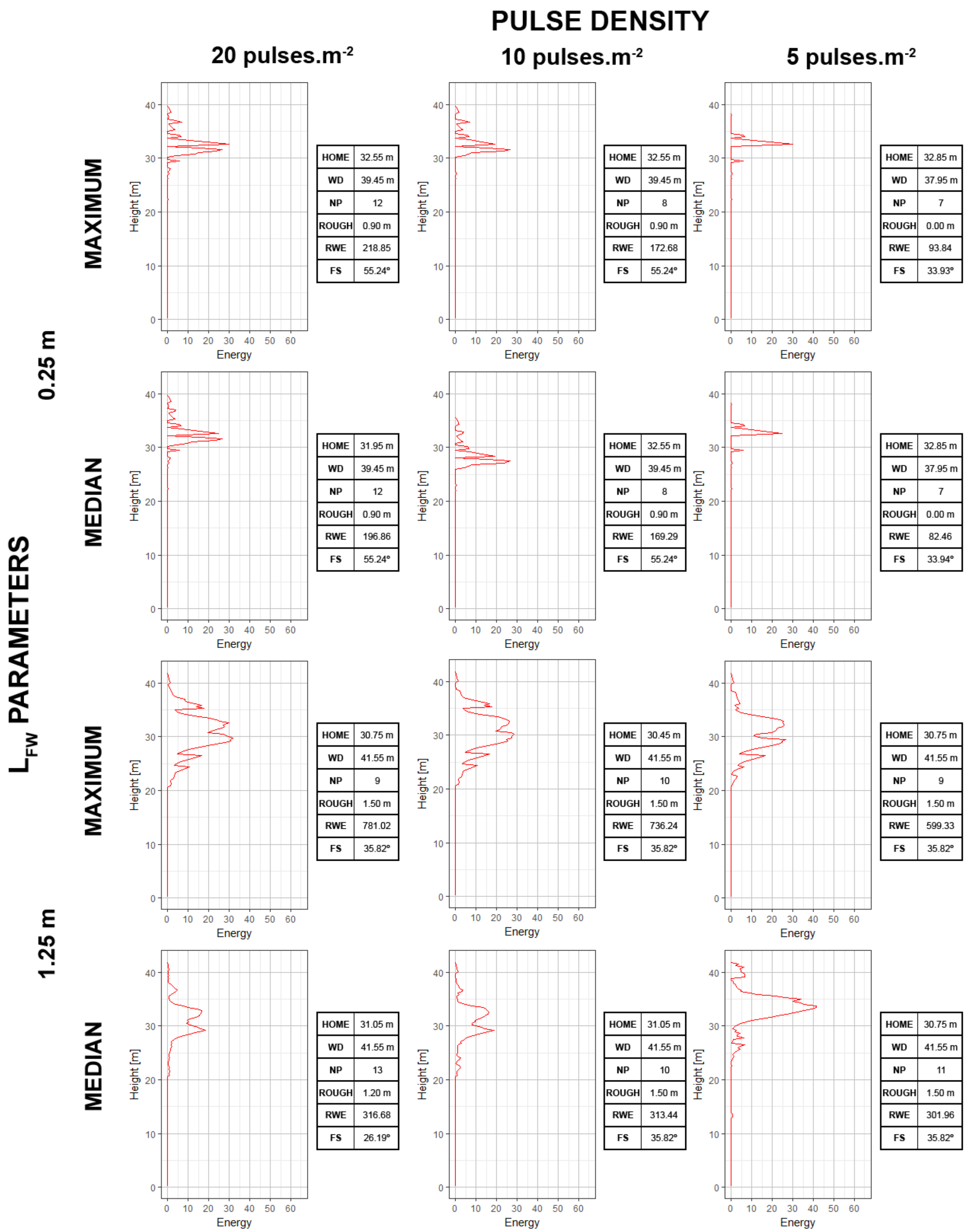

Fig. 3. Examples of pseudo-vertical waveforms at voxel column-level and L_{FW}-derived metric values for different pulse densities (20, 10 and 5 pulses·m^{-2}), voxel sizes (0.25 and 1.25 m) and assignation values (maximum and median).

3.1. Analysis of L_{FW}-derived metric variation related to pulse density

Fig. 4 shows the variation of HOME in one sample for the different pulse densities with the maximum assignation and voxel sizes of 0.25 and 0.75 m. In the case of 0.25 m (Fig. 4a), the trend fits a negative exponential model. This does not occur using a voxel size of 0.75 m (Fig. 4b). The negative exponential function shows that HOME values progressively increase as pulse density increases, until they reach the sill of the curve at 9-10 pulses·m^{-2} (in this case the MPD was 7.11 pulses·m^{-2}). However, HOME values in Fig. 4b, except for a pulse density of 2 pulses·m^{-2}, seem to be constant, even with a slight negative slope. This negative slope prevents from the fitting with a negative exponential model.

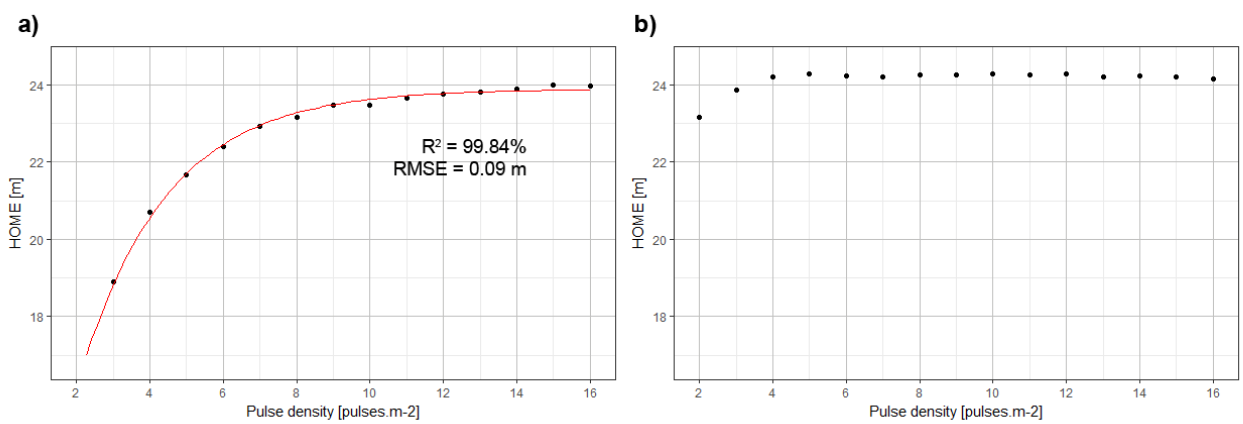

Fig. 4. Variation of HOME related to pulse density in one sample for the maximum assignation value and voxel sizes of (a) 0.25 m and (b) 0.75 m. The black points represent the values computed and the red curve the fitted model, being (a) negative exponential. The values of HOME in (b) do not fit a negative exponential model.

After generating the fitted models for every sample, Fig. 5a shows the average of the adjusted MPD values from the 30 samples where the corresponding L_{FW}-derived metric remains stable (i.e., the *b* coefficients from the negative exponential models (see Eq. (2))); and Fig. 5b shows the standard deviation of the MPD for all samples. All the models obtained a Jackknife bias lower than $1.56 \cdot 10^{-13}$ in the validation procedure for the three coefficients of the negative exponential model (e.g. a, b, and c). This means that there were not outliers after applying the leave-one-out procedure. It is important to remark that negative exponential models were generated using sample data from 2 to 16 pulses$\cdot$m^{-2}. Hence, L_{FW}-derived metric variation values estimated out of this range are extrapolations, and as such the resulting MPD values higher than 16 pulses$\cdot$m^{-2} must be considered carefully. Additionally, empty cells in Fig. 5 correspond to combinations of metrics and voxel sizes that do not fit a negative exponential model. NP, ROUGH and RWE are the metrics with highest MPD values (MPD ϵ [42.2, 46.2], MPD ϵ [18.7, 21.3] and MPD ϵ [60.2, 89.7] pulses$\cdot$m^{-2}, respectively, for a voxel size of 0.25 m), while HOME, WD and FS have the lowest (MPD ϵ [7.1, 7.2], MPD = 9.6 and MPD ϵ [3.9, 4.1] pulses$\cdot$m^{-2}, respectively, for a voxel size of 0.25 m). Every L_{FW}-derived metric remains asymptotically stable at lower pulse densities as voxel size increases. For instance, the MPD decreases from 7.1 to 3.4 pulses$\cdot$m^{-2} for HOME; from 9.6 to 8.4 pulses$\cdot$m^{-2} for WD; from 45.5 to 15.4 pulses$\cdot$m^{-2} for NP; from 21 to 4.6 pulses$\cdot$m^{-2} for ROUGH; and from 60.2 to 5.3 pulses$\cdot$m^{-2} for RWE. However, WD has low values for voxel sizes of 0.35 and 0.45 m (MPD ϵ [8.4, 8.5]), but they increase again as the voxel size also increases (MPD = 13.5 pulses$\cdot$m^{-2}). Results also show that for low MPD values (i.e. MPD ϵ [3.9, 5.6]), L_{FW}-derived metric variation does not fit a negative exponential trend for high voxel sizes. This behavior is observed with HOME, ROUGH, RWE and FS, except for ROUGH using the maximum assignation value. In these cases, L_{FW}-derived metric values tend to slightly decrease as pulse density increases.

Comparing different assignation values, HOME, WD, NP and FS have similar MPD values; however, ROUGH and RWE were influenced differently. Both ROUGH and RWE remain stable at lower pulse densities using the median as assignation value, but they present more variation using the maximum, percentiles 90 and 95. For instance, RWE has a MPD value of 5.3 pulses·m^{-2} using the median assignation and a voxel size of 1.25 m, while the MPD value was 18.6 using the maximum and the same voxel size.

Analyzing the average of the standard deviation of the MPD from the 30 samples (Fig. 5b), all the values are low (between 1 and 2.6 pulses·m^{-2}) except for NP and RWE with small voxel sizes. These L_{FW}-derived metrics have large standard deviations for small voxel sizes ([6.7, 8.6] and [5.8, 11] pulses·m^{-2}, respectively), diminishing the values for larger voxel sizes ([1.9, 2.3] and [1.0, 1.2] pulses·m^{-2}, respectively). However, the standard deviation of ROUGH using the maximum assignation increases as voxel size increases. High standard deviation values of MPD are related to high MPD values.

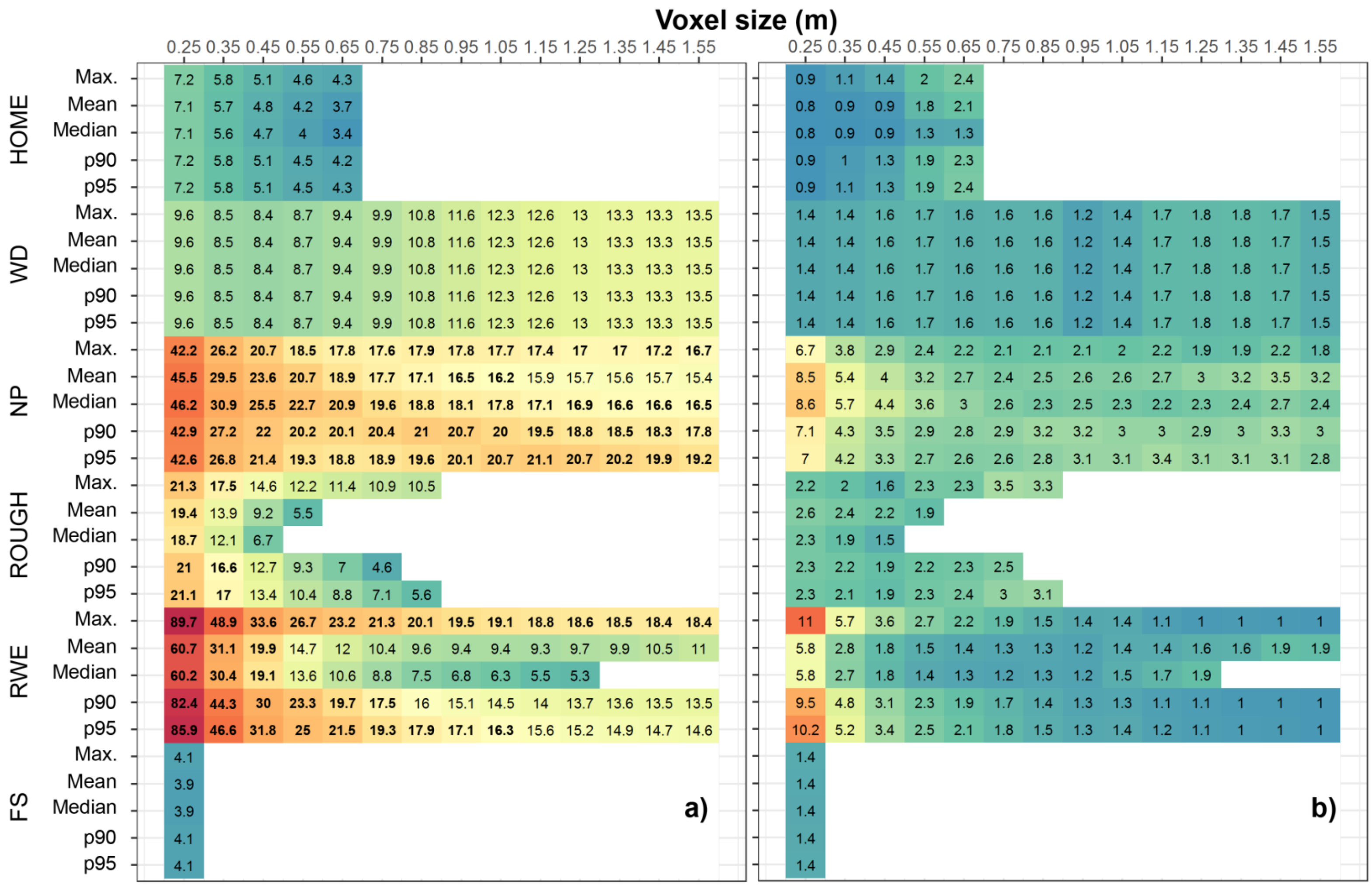

Fig. 5. (a) Average minimum pulse density (MPD; i.e. coefficient b from the negative exponential model) from the 30 samples for different voxel sizes and assignation values. Empty cells correspond to combinations of metrics and voxel sizes that do not fit a negative exponential model. Values in bold correspond to MPD values higher than 16 pulses·m^{-2} (i.e. the maximum pulse density from sample data used to generate the negative exponential model). (b) Average standard deviation of MPD for the 30 samples tested. Smallest and highest values are represented by blue and red colors, respectively.

3.2. Analysis of L_{FW}-derived metric variation related to voxel size and assignation value

Fig. 6 shows the Total Variation standardized (TVar) value defined by Eq. (3) and (4) for every L_{FW}-derived metric computed at the different voxel sizes and assignation values. Overall, HOME, WD and FS present the lowest TVar values (TVar $\in$ [0.03, 0.27], TVar $\in$ [0.06, 0.28] and TVar $\in$ [0.10, 0.28], respectively), while NP, ROUGH and RWE present higher values (TVar $\in$ [0.24, 0.36], TVar $\in$ [0.14, 0.52] and TVar $\in$ [0.012, 0.45], respectively, using small voxel sizes). TVar values of HOME, WD, NP for maximum, RWE for mean and median, and FS, decrease as voxel size increases compared to the lowest voxel size (i.e. 0.25 m). These values range from 0.27 to 0.04 for HOME, from 0.28 to 0.06 for WD, from 0.33 to 0.30 for NP with the maximum assignation value; from [0.40, 0.45] to [0.12, 0.17] for RWE with the mean and median assignation values; and from [0.26, 0.28] to [0.10, 0.14] for FS. NP TVar values do not vary significantly as voxel size increases, the values being [0.24, 0.32] at 0.25 m, and [0.27, 0.30] the lowest TVar values at other voxel sizes. Regarding RWE, the TVar values are minimal at the lowest voxel size using the maximum, percentiles 90 and 95 as assignation values. Nevertheless, TVar values are particularly high at the lowest voxel size using the mean and median assignation value, and become low for the largest voxel sizes, especially with the median. In addition, TVar values from ROUGH steeply increase as voxel size increases, varying from [0.14, 0.23] at 0.25 m to [0.38, 0.52] at 1.55 m.

Regarding the assignation values, HOME and WD present little or no differences. However, NP, ROUGH and RWE have different TVar values depending on the assignation values. NP has the lowest value at 0.25 m for the median assignation value (TVar = 0.24). The lowest TVar values of ROUGH are reached using the maximum, percentiles 90 and 95. Finally, RWE TVar values have the largest differences between assignation values, the mean and median being completely different from the others.

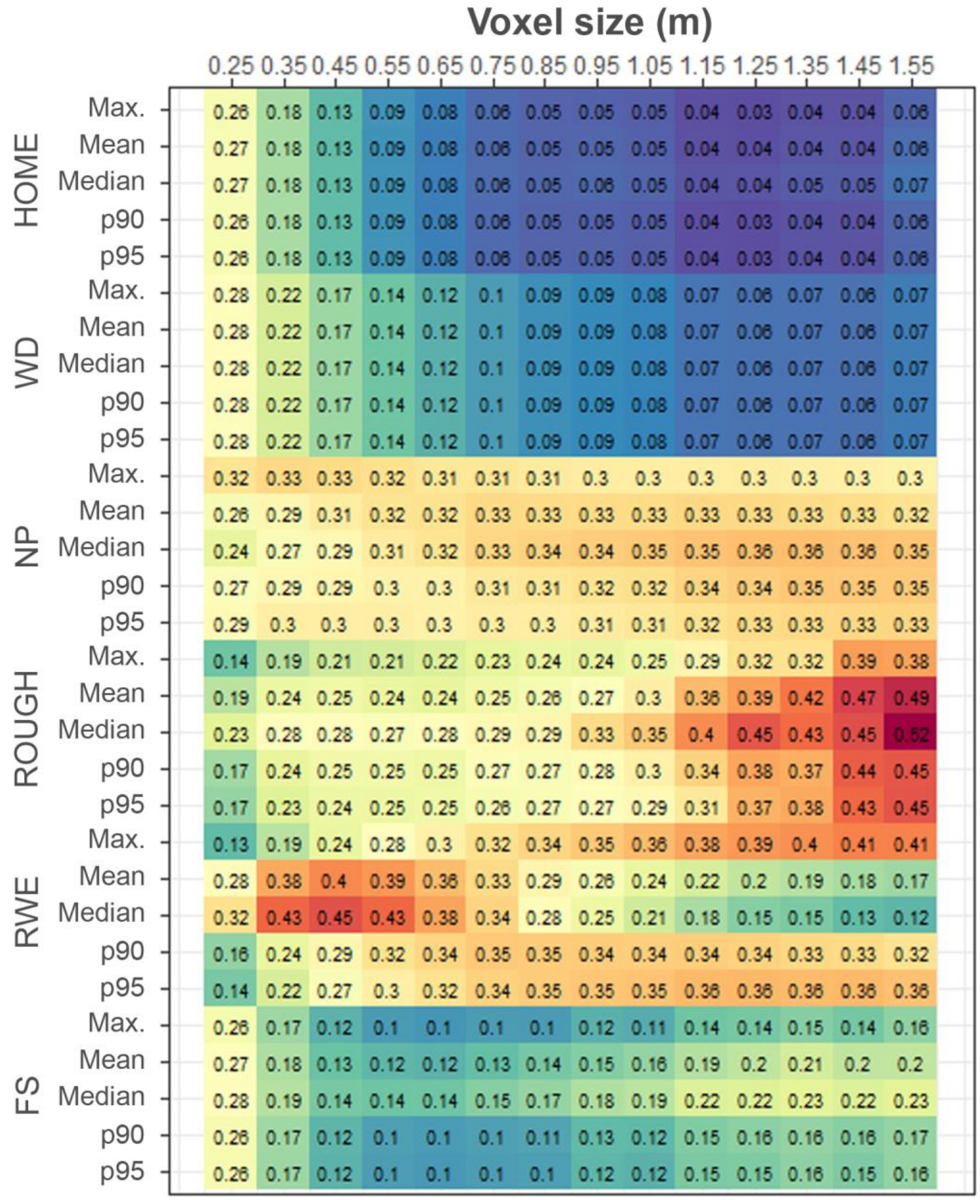

Fig. 6. Total Variation values for the different L_{FW}-derived metrics computed for the assignation values and voxel sizes. Smallest and highest values are represented by blue and red colors, respectively.

4. Discussion

In this research we analyzed how L_{FW}-derived metrics varied according to pulse density, voxel size and assignation value. Key results indicate that L_{FW}-derived metric variations due to pulse density differences can be modelled, and therefore their impact reduced by setting a MPD, modifying the voxel size and/or the assignation value used. This may help to diminish the side-lap effect in a particular study area, and therefore to obtain a more accurate estimate of forest stand variables.

Results showed that L_{FW}-derived metric variations related to pulse density have a negative exponential behavior, especially with small voxel sizes. Usually, there is a MPD from which metric values are stabilized. In new L_{FW} acquisitions, this MPD should be the minimum pulse density value registered by the sensor to avoid the side-lap effect. However, the MPD is not constant for every L_{FW}-derived metric, voxel size or assignation values employed. Therefore, in practice, either the most affected L_{FW}-derived metrics should be avoided for estimation of forest stand variables, the voxel size increased or the assignation value modified.

On the other hand, when L_{FW} has already been acquired, pulse density cannot be increased, and therefore other strategies are required, such as modifying L_{FW} parameters. Our results showed that increasing the voxel size and/or modifying the assignation value can make more stable L_{FW}-derived metrics. The probability that larger voxels are crossed by at least one waveform is higher, avoiding the gaps in the voxel columns that may alter L_{FW}-derived metric values. Eventually, a trade-off between increasing voxel size to reduce side-lap effect and a substantial loss of resolution should be considered. Regarding the assignation value, its effect on the stability of L_{FW}-derived metrics depends on the chosen metrics. Some standard L_{FW}-derived metrics, such as RWE, have unstable behavior, whereas some others, such as WD, have not. In general, the increment of the voxel size and the change of the assignation value reduce the L_{FW}-derived metric variation.

MPD values determine the minimum pulse density required to obtain stable L_{FW}-derived metrics. However, the variation trend of some L_{FW}-derived metrics does not follow a negative exponential model. Additionally, in some metrics (e.g. WD) higher values of MPD do not correspond to higher values of TVar. Therefore, the introduction of TVar complements the MPD as an indicator of the variability of the L_{FW}-derived metric due to pulse density changes.

Regarding different behavior among L_{FW}-derived metrics, NP and RWE are more sensitive to pulse density changes than the rest. The lack of one or more voxel values means fewer peaks and a different sum of amplitudes in the wave. On the contrary, HOME, WD, ROUGH (at lower voxel sizes) and FS are less affected, since they are metrics that are related either to the height or to the top texture of the canopy, where the laser energy from airborne sensors arrives without occlusion (Crespo-Peremarch and Ruiz, 2017). WD only requires a proper estimation of the height of the beginning of the waveform (top of the canopy), and it is well determined if the waveform intersects with the top of the trees. HOME calculation involves the beginning of the waveform as well as the height of the median energy. The latter is usually well registered, since it often corresponds to the densest vertical layer (see HOME values in Fig. 3). ROUGH and FS calculation requires the beginning of the waveform, and the position and amplitude of the first peak. Therefore, HOME, WD, ROUGH and FS vary if some voxel columns have no data due to a low pulse density. In order to avoid this, an increment of the voxel size is required.

In addition, there is remarkable disparity in L_{FW}-derived metric values using different assignation values. MPD and TVar values from WD do not vary, since the beginning of the waveform does not vary by modifying the assignation value. HOME has slight differences, since the height of the median energy may vary depending on the assignation employed. NP also presents minor variation, since the pseudo-vertical waveform has more singularities when the maximum assignation value is employed. ROUGH also has some differences due to possible variations of the first peak. RWE is the most variable L_{FW}-derived metric. As it is computed as the sum of amplitudes of a waveform, the sum of maximum values may substantially differ from the sum of median values, for instance. A normalized metric may be used in order to avoid these differences. A possible approach could be to calculate a normalized RWE (nRWE) following Eq. (4), where x is equal to RWE, and min(x) and max(x) are the minimum and maximum RWE values, respectively, for each assignation value. Thus, nRWE values from different assignation values would be comparable. Finally, FS may present small differences, since the amplitude and position of the first peak can vary as well.

To summarize, in order to reduce the side-lap effect in this scenario, the increment of the voxel size is recommended for HOME, WD, FS, and RWE for the mean and median assignation values, but not for ROUGH and RWE when maximum, percentiles 90 and 95 assignation values are used. Besides, depending on the voxel size, the selection of the assignation value has to be considered for RWE. According to results, NP might be discarded for estimating forest stand variables because of its sensitivity to pulse density. Observing Figures 5 and 6, MPD, voxel size and assignation values can be selected to minimize the side-lap effect in areas with similar vegetation types and densities. When planning a LiDAR flight, a MPD around 10 pulses·m^{-2}, a voxel size of 0.75 m or similar, and the mean or median voxel assignation seem to optimize general performance. This combination of parameters provides the minimum values of MPD for most of the L_{FW}-derived metrics (Fig. 5), except for NP. However, if LiDAR data are already available and the pulse density cannot be increased, the maximum assignation and a voxel size of about 0.75 m would be the most efficient option in terms of reduction of side-lap effect (Fig. 6).

There are few published studies that analyze how L_{FW}-derived metrics respond to progressive variations of the LiDAR pulse density. Crespo-Peremarch et al. (2016) analyzed differences in L_{FW}-derived metrics between pair samples with similar (but not identical) forest structure and different pulse densities due to side-lap effect. They employed a paired Student's t-test and the Wilcoxon signed-rank test to determine whether L_{FW}-derived metrics were significantly different between pair samples, quantifying these differences. Although general conclusions were reached in this study, they do not allow for a practical treatment of the problem. Nevertheless, the behavior of the metrics related to pulse density variations has been analyzed in more detail and with greater sensitivity. For instance, the definition and use of MPD and TVar provides more complete information about L_{FW}-derived metric variations, since they were measured in the same sample but with different pulse density, as well as practical guidance to reduce the effect of density differences in L_{FW} data sets.

Our results are analogous to those of previous studies using L_D. In these studies, a similar tendency for R^2 (Jakubowski et al., 2013; Manuri et al., 2017), reliability ratio (Magnussen et al., 2010; Hansen et al., 2015) and maximum height metric (Roussel et al., 2017) was found. These values stabilize as pulse density increases.

Modelling L_{FW}-derived metric variations related to the pulse density is relevant to remove or reduce the side-lap effect when mapping metrics and forest structural variables are computed. Depending on the LiDAR data acquisition step, different strategies can be followed. First, if L_{FW} data has not been acquired yet, a minimum pulse density that keeps L_{FW}-derived metrics stable may be set. Second, if L_{FW} data has already been acquired, L_{FW}-derived metric variation can be reduced by increasing the voxel size to a certain extent, and/or using a specific assignation value. In this case, the pulse density cannot be increased, therefore L_{FW} parameters that provide more stable metrics should be used. Finally, if some variables do not respond to these strategies and reducing the side-lap effect is not possible, then they should be avoided for further analyses.

5. Conclusions

The present study has analyzed the variation of L_{FW}-derived metrics according to the pulse density. This variation is common due to side-lap areas that are registered with a higher pulse density, and is known as “side-lap effect”. Our results suggest that L_{FW}-derived metric variations related to pulse density can be modelled in most cases using a negative exponential model, and therefore there is a threshold at which their values stabilize. From this point, a minimum pulse density can be set to avoid the side-lap effect. In addition, modifying L_{FW} parameters (i.e. voxel size and assignation value) reduces the side-lap effect when pulse density cannot be increased, e.g. when L_{FW} data has already been acquired. Thus, an increment of the voxel size is recommended for HOME, WD, FS and RWE for the mean and median assignation values. Nevertheless, small voxel sizes make ROUGH and RWE for maximum, percentiles 90 and 95 more stable. On the other hand, the choice of the assignation value must be considered depending on the voxel size used for RWE. However, NP is sensitive to pulse density variations and they cannot be reduced through L_{FW} parameters, and therefore should be avoided for further analyses. The results presented in this study have practical relevance in order to avoid the side-lap effect when estimating forest stand variables using L_{FW} data. Further studies could focus on analyzing the effect of these parameters on different ecosystems with different dominant species, as well as the effect of the emitted pulse energy and footprint size on L_{FW}-derived metrics, since they also influence the penetration of laser pulses.

6. Acknowledgments

This research has been funded by the Spanish Ministerio de Economía y Competitividad and FEDER, in the framework of the project CGL2016-80705-R. The authors also thank the Bureau of Land Management and the Panther Creek Remote Sensing and Research Cooperative Program for the data provided.

7. References

Bailey, R.G., 1980. Description of the ecoregions of the United States. 2nd edition USDA Forest Service, Miscellaneous Publication 1391 (Washington, DC).

Bortolot, Z.J., Wynne, R.H., 2005. Estimating forest biomass using small footprint LiDAR data: An individual tree-based approach that incorporates training data. ISPRS Journal of

Photogrammetry and Remote Sensing. 59(6), 342-360. https://doi.org/10.1016/j.isprsjprs.2005.07.001

Cao, L., Coops, N.C., Hermosilla, T., Innes, J., Dai, J., She, G., 2014. Using small-footprint discrete and full-waveform airborne LiDAR metrics to estimate total biomass and biomass components in subtropical forests. Remote Sensing. 6(8), 7110-7135. https://doi.org/10.3390/rs6087110

Cao, L., Coops, N.C., Innes, J.L., Dai, J., Ruan, H., She, G., 2016. Tree species classification in subtropical forests using small-footprint full-waveform LiDAR data. International Journal of Applied Earth Observation and Geoinformation. https://doi.org/10.1016/j.jag.2016.01.007

Crespo-Peremarch, P., Ruiz, L.A., Balaguer-Beser, A., Estornell, J., 2016. Analysis of the side-lap effect on full-waveform LiDAR data acquisition for the estimation of forest structure variables. ISPRS-International Archives of the Photogrammetry, Remote Sensing and Spatial Information Sciences. 41, 603-610. https://doi.org/10.5194/isprs-archives-xli-b8-603-2016

Crespo-Peremarch, P., Ruiz, L.A., 2017. Análisis comparativo del potencial del ALS y TLS en la caracterización estructural de la masa forestal basado en voxelización. XVII Congreso de la Asociación Española de Teledetección, Nuevas plataformas y sensores de teledetección. 131-135.

Crespo-Peremarch, P., Ruiz, L.A., 2018. Influence of lidar full-waveform density and voxel size on forest stand estimates. IGARSS 2018 (International Geoscience and Remote Sensing Symposium), Observing, Understanding and Forecasting the Dynamics of Our Planet.

David, M., 1977. Geostatistical ore reserve estimation, Elsevier, Amsterdam, The Netherlands. https://doi.org/10.1016/c2009-0-14528-2

Duda, R.O., Hart, P.E., Stork, D.G., 2012. Pattern classification. John Wiley & Sons.

Duong, V.H., 2010. Processing and application of ICESat large footprint full waveform laser range data (Doctoral dissertation, TU Delft, Delft University of Technology).

Gobakken, T., Naesset, E., 2008. Assessing effects of laser point density, ground sampling intensity, and field sample plot size on biophysical stand properties derived from airborne laser scanner data. Canadian Journal of Forest Research. 38(5), 1095-1109. https://doi.org/10.1139/x07-219

González-Ferreiro, E., Diéguez-Aranda, U., Miranda, D., 2012. Estimation of stand variables in Pinus radiata D. Don plantations using different LiDAR pulse densities. Forestry. 85(2), 281-292. https://doi.org/10.1093/forestry/cps002

Guerra-Hernández, J., Tomé, M., González-Ferreiro, E., 2016. Using low density LiDAR data to map Mediterranean forest characteristics by means of an area-based approach and height threshold analysis. Revista de Teledetección. 0(46), 103-117. https://doi.org/10.4995/raet.2016.3980

Guo, L., Chehata, N., Mallet, C., Boukir, S., 2011. Relevance of airborne lidar and multispectral image data for urban scene classification using Random Forests. ISPRS Journal of Photogrammetry and Remote Sensing. 66(1), 56-66. https://doi.org/10.1016/j.isprsjprs.2010.08.007

Hansen, E.H., Gobakken, T., Naesset, E., 2015. Effects of pulse density on digital terrain models and canopy metrics using airborne laser scanning in a tropical rainforest. Remote Sensing. 7(7), 8453-8468. https://doi.org/10.3390/rs70708453

Harten, A., 1983. High resolution schemes for hyperbolic conservation laws. Journal of Computational Physics. 49(3), 357-393. https://doi.org/10.1016/0021-9991(83)90136-5

Heinzel, J., Koch, B., 2011. Exploiting full-waveform LiDAR parameters for tree species classification. International Journal of Applied Earth Observation and Geoinformation. 13(1), 152-160. https://doi.org/10.1016/j.jag.2010.09.010

Hermosilla, T., Ruiz, L.A., Kazakova, A.N., Coops, N.C., Moskal, L.M., 2014a. Estimation of forest structure and canopy fuel parameters from small-footprint full-waveform LiDAR data. International Journal of Wildland Fire. 23(2), 224-233. https://doi.org/10.1071/wf13086

Hermosilla, T., Coops, N.C., Ruiz, L.A., Moskal, L.M., 2014b. Deriving pseudo-vertical waveforms from small-footprint full-waveform LiDAR data. Remote Sensing Letters. 5(4), 332-341. https://doi.org/10.1080/2150704x.2014.903350

Hevia, A., Álvarez-González, J., Ruiz-Fernández, E., Prendes, C., Ruiz-González, A., Majada, J., González-Ferreiro, E., 2016. Modelling canopy fuel and forest stand variables and characterizing the influence of thinning in the stand structure using airborne LiDAR. Revista de Teledetección. 0(45), 41-55. https://doi.org/10.4995/raet.20163979

Jakubowski, M.K., Guo, Q., Kelly, M., 2013. Tradeoffs between lidar pulse density and forest measurement accuracy. Remote Sensing of Environment. 130, 245-253. https://doi.org/10.1016/j.rse.2012.11.024

Kashani, A.G., Olsen, M.J., Parrish, C.E., Wilson, N., 2015. A review of LiDAR radiometric processing: From ad hoc intensity correction to rigorous radiometric calibration. Sensors. 15(11), 28099-28128. https://doi.org/10.3390/s151128099

Kukko, A., Kaasalainen, S., Litkey, P., 2008. Effect of incidence angle on laser scanner intensity and surface data. Applied Optics. 47(7), 986-992. https://doi.org/10.1364/ao.47.000986

Lefsky, M.A., Harding, D.J., Keller, M., Cohen, W.B., Carabajal, C.C., Del Bom Espirito-Santo, F., Hunter, M.O., de Oliveira Jr., R., 2005. Estimates of forest canopy height and aboveground biomass using ICESat. Geophysical Research Letters. 32(22). https://doi.org/10.1029/2005gl023971

Lim, K., Treitz, P., Wulder, M., St-Onge, B., Flood, M., 2003. LiDAR remote sensing of forest structure. Progress in Physical Geography. 27(1), 88-106.

Magnussen, S., Naesset, E., Gobakken T., 2010. Reliability of LiDAR derived predictors of forest inventory attributes: A case study with Norway spruce. Remote Sensing of Environment. 114(4), 700-712. https://doi.org/10.1016/j.rse.2009.11.007

Mallet, C., Bretar, F., 2009. Full-waveform topographic lidar: State-of-the-art. ISPRS Journal of Photogrammetry and Remote Sensing. 64(1), 1-16. https://doi.org/10.1016/j.isprsjprs.2008.09.007

Manuri, S., Andersen, H.E., McGaughey, R.J., Brack, C., 2017. Assessing the influence of return density on estimation of lidar-based aboveground biomass in tropical peat swamp forests of Kalimantan, Indonesia. International Journal of Applied Earth Observation and Geoinformation. 56, 24-35. https://doi.org/10.1016/j.jag.2016.11.002

Mutlu, M., Popescu, S.C., Stripling, C., Spencer, T., 2008. Mapping surface fuel models using lidar and multispectral data fusion for fire behavior. Remote Sensing of Environment. 112(1), 274-285. https://doi.org/10.1016/j.rse.2007.05.005

Reitberger, J., Krzystek, P., Stilla, U., 2008. Analysis of full waveform LiDAR data for the classification of deciduous and coniferous trees. International Journal of Remote Sensing. 29(5), 1407-1431. https://doi.org/10.1080/01431160701736448

Reitberger, J., Schnörr, C., Krzystek, P., Stilla, U., 2009. 3D segmentation of single trees exploiting full waveform LiDAR data. ISPRS Journal of Photogrammetry and Remote Sensing. 64(6), 561-574. https://doi.org/10.1016/j.isprsjprs.2009.04.002

Roussel, J.R., Caspersen, J., Béland, M., Thomas, S., Achim, A., 2017. Removing bias from LiDAR-based estimates of canopy height: accounting for the effects of pulse density and footprint size. Remote Sensing of Environment. 198, 1-16. https://doi.org/10.1016/j.rse.2017.05.032

Ruiz, L.A., Hermosilla, T., Mauro, F., Godino, M., 2014. Analysis of the influence of plot size and LiDAR density on forest structure attribute estimates. Forests. 5(5), 936-951. https://doi.org/10.3390/f5050936

Ruiz, L.A., Recio, J.A., Crespo-Peremarch, P., Sapena, M., 2018. An object-based approach for mapping forest structural types based on low-density LiDAR and multispectral imagery. Geocarto International. 33(5), 443-457. https://doi.org/10.1080/10106049.2016.1265595

Silva, C.A., Hudak, A.T., Klauberg, C., Vierling, L.A., Gonzalez-Benecke, C., Carvalho, S.D.P.C., Rodriguez, L.C.E., Cardil, A., 2017. Combined effect of pulse density and grid cell size on predicting and mapping aboveground carbon in fast-growing Eucalyptus forest plantation using airborne LiDAR data. Carbon Balance and Management. 12(1), 13. https://doi.org/10.1186/s13021-017-0082-0

Song, J.H., Han, S.H., Yu, K.Y., Kim, Y.I., 2002. Assessing the possibility of land-cover classification using lidar intensity data. International Archives of Photogrammetry Remote Sensing and Spatial Information Sciences. 34(3/B), 259-262.

Strunk, J., Temesgen, H., Andersen, H.E., Flewelling, J.P., Madsen, L., 2012. Effects of lidar pulse density and sample size on a model-assisted approach to estimate forest inventory variables. Canadian Journal of Remote Sensing. 38(5), 644-654. https://doi.org/10.5589/m12-052

Treitz, P., Lim, K., Woods, M., Pitt, D., Nesbitt, D., Etheridge, D., 2012. LiDAR sampling density for forest resource inventories in Ontario, Canada. Remote Sensing. 4(4), 830-848. https://doi.org/10.3390/rs4040830

Varo-Martínez, M.Á., Navarro-Cerrillo, R.M., Hernández-Clemente, R., Duque-Lazo, J., 2017. Semi-automated stand delineation in Mediterranean *Pinus sylvestris* plantations through segmentation of LiDAR data: The influence of pulse density. International Journal of Applied Earth Observation and Geoinformation. 56, 54-64. https://doi.org/10.1016/j.jag.2016.12.002

Wagner, W., 2010. Radiometric calibration of small-footprint full-waveform airborne laser scanner measurements: Basic physical concepts. ISPRS Journal of Photogrammetry and Remote Sensing. 65(6), 505-513. https://doi.org/10.1016/j.isprsjprs.2010.06.007